AIP | The Journal of Chemical Physics

Coarse-grained simulations for flow of complex soft matter fluids in the bulk and in the presence of solid interfaces

V. R. Ahuja, J. van der Gucht, and W. J. Briels

Citation: The Journal of Chemical Physics **145**, 194903 (2016); doi: 10.1063/1.4967422
View online: http://dx.doi.org/10.1063/1.4967422
View Table of Contents: http://scitation.aip.org/content/aip/journal/jcp/145/19?ver=pdfcov
Published by the AIP Publishing

Coarse-grained simulations for flow of complex soft matter fluids in the bulk and in the presence of solid interfaces

V. R. Ahuja,[1,2,3,a)] J. van der Gucht,[3] and W. J. Briels[1,2,4,a)]
[1]*Computational Chemical Physics, Faculty of Science and Technology, University of Twente, P.O. Box 217, 7500 AE Enschede, The Netherlands*
[2]*MESA+ Institute for Nanotechnology, University of Twente, P.O. Box 217, 7500 AE Enschede, The Netherlands*
[3]*Physical Chemistry and Soft Matter, Wageningen University, Helix, Building 124, Stippeneng 4, 6708 WE Wageningen, The Netherlands*
[4]*Forschungszentrum Jülich, ICS 3, D-52425 Jülich, Germany*

(Received 6 September 2016; accepted 27 October 2016; published online 16 November 2016)

We present a coarse-grained particle-based simulation technique for modeling flow of complex soft matter fluids such as polymer solutions in the presence of solid interfaces. In our coarse-grained description of the system, we track the motion of polymer molecules using their centers-of-mass as our coarse-grain co-ordinates and also keep track of another set of variables that describe the background flow field. The coarse-grain motion is thus influenced not only by the interactions based on appropriate potentials used to model the particular polymer system of interest and the random kicks associated with thermal fluctuations, but also by the motion of the background fluid. In order to couple the motion of the coarse-grain co-ordinates with the background fluid motion, we use a Galilean invariant, first order Brownian dynamics algorithm developed by Padding and Briels [J. Chem. Phys. **141**, 244108 (2014)], which on the one hand draws inspiration from smoothed particle hydrodynamics in a way that the motion of the background fluid is efficiently calculated based on a discretization of the Navier-Stokes equation at the positions of the coarse-grain coordinates where it is actually needed, but also differs from it because of the inclusion of thermal fluctuations by having momentum-conserving pairwise stochastic updates. In this paper, we make a few modifications to this algorithm and introduce a new parameter, viz., a friction coefficient associated with the background fluid, and analyze the relationship of the model parameters with the dynamic properties of the system. We also test this algorithm for flow in the presence of solid interfaces to show that appropriate boundary conditions can be imposed at solid-fluid interfaces by using artificial particles embedded in the solid walls which offer friction to the real fluid particles in the vicinity of the wall. We have tested our method using a model system of a star polymer solution at the overlap concentration. *Published by AIP Publishing.* [http://dx.doi.org/10.1063/1.4967422]

I. INTRODUCTION

The flow of complex soft matter involving mesoscopic particles can be described, in principle, by simultaneously solving the coupled deterministic equations of motion of all the atoms present in the system.[1,2] However, when dealing with processes occurring in soft matter systems over substantially longer length and time scales, typically several orders of magnitude higher than those occurring at the atomic level, this becomes computationally very expensive, rendering it practically impossible to solve the problem in this manner in a reasonable time-frame even with the state-of-the-art computers available today. Therefore, a computationally efficient solution is to simplify the description by lumping groups of atoms into coarse-grain sites which then interact with each other through effective interactions, thereby integrating out several internal degrees of freedom and making the problem tractable.[3,4] Although it might seem too simplistic, it is interesting to notice that several phenomena in complex soft matter systems such as polymer melts, polymer solutions, and worm-like-micellar solutions have actually been studied by restricting the focus just to the motion of the centers-of-mass of the mesoscopic particles therein.[5–10] It is needless to say that one has to be conscious of the fact that when modeling a system with coarse-grain simulations using the positions of the centers-of-mass, several internal degrees of freedom have been eliminated, which need to be accounted for. For instance, the same set of positions of these centers-of-mass could have a different time evolution because of a different configuration of the eliminated degrees of freedom. Hence, the coarse-grain system can no longer be treated as deterministic. This can be achieved by updating the positions of the centers-of-mass of the mesoscopic particles through a stochastic differential equation such as Langevin or Brownian dynamics.

At the outset, we would like to clarify what we refer to as Langevin and Brownian dynamics throughout this paper. According to the terminology that we have employed, the motion of a mesoscopic particle moving through a stationary background according to Langevin dynamics is given by a second-order stochastic differential equation where the total force acting on the mesoscopic particle is given by a sum

a)Authors to whom correspondence should be addressed. Electronic addresses: v.r.ahuja@utwente.nl and w.j.briels@utwente.nl

of three forces, viz., a driving force due to the interaction with other mesoscopic particles or an external force field, a frictional force proportional to the velocity of the particle but acting against it, and a random force, whose properties are calculated based on the fluctuation dissipation theorem, thereby serving as a thermostat. Dissipative Particle Dynamics (DPD),[11–13] for instance, uses a framework based on Langevin dynamics. However, for highly overdamped soft matter systems, where friction coefficients are large, the time scale over which the velocities get thermalized is much shorter than the time scale over which the positions of the particles change to any significant extent. In such cases, one can average over the velocities and use instead a first order stochastic differential equation to update the position of the particles, henceforth referred to as Brownian dynamics.[14,15] Several phenomena in soft matter systems, ranging from viscoelasticity in polymer solutions, shear thinning behavior, alignment of colloids in viscoelastic fluids, dynamics of proteins, etc., have been studied using a framework based on Brownian dynamics or its variations.[8–10,16–20]

In order to study flow behavior of soft matter systems, the standard Brownian dynamics equations must be modified by the addition of a term that accounts for the velocity of the background material so that the friction is applied to the motion of the particles relative to the background velocity field. It is straightforward to do this if the background flow field is known *a priori*. However, for flows of soft matter systems through complex geometries involving solid interfaces, the flow field can be very complex and is not known *a priori*. The velocity of the background material at the position of the particle may be computed by averaging the drift velocity of the other particles in the vicinity of the particle itself. This has been done previously for the special case of shear flow of soft matter systems, where the velocity of the background material was calculated by spatio-temporally averaging the velocity of the particles in flow-oriented layers to study shear banding.[21–25]

A more general momentum-conserving algorithm for modeling self-developing flows of complex fluids in any flow situation has been developed recently.[26] Using this algorithm, friction is applied to the relative motion of the coarse-grained particles with respect to the background fluid. A separate set of variables is used for describing the background fluid velocities, which are updated based on a discretization of the Navier-Stokes equation at the positions of the coarse-grain coordinates, in a way similar to Smoothed Particle Hydrodynamics (SPH).[27–31] This obviates the need to calculate the entire background flow field and instead calculates the flow field only at the positions of the coarse-grain coordinates, where it is actually needed. The background velocity at the position of a coarse-grained particle is also influenced by the forces acting on the coarse-grained particle due to its interaction with other coarse-grained particles in its vicinity. These forces are immediately transmitted to the background flow field using a friction coefficient associated with the background fluid, which is an additional parameter we have introduced in the algorithm; however, the background material retains memory of this force, which gradually fades away with a characteristic time constant. The characteristic time constant and the friction coefficients are input parameters for our simulations which can, in principle, be calculated from the physical properties of the system measured experimentally or obtained from independent simulations. The friction coefficient associated with the coarse-grain motion may be calculated from the diffusion coefficient of the particles in the system. In this paper, however, since the focus is model development, we have not used real values obtained from experimental data of physical properties but rather non-dimensionalized our results with respect to a basis set.

Since the motion of the coarse-grain particles influences the background flow field by transmitting the inter-particle force to it and the background flow field in turn influences the frictional force offered to the coarse-grain particles, this is a two-way coupling algorithm. In other words, the information about the background flow field is obtained effectively by spatio-temporally averaging the velocities in the vicinity of the coarse-grain coordinates, which is then used to calculate the friction for these coarse-grained particles relative to this background flow field. Furthermore, the background velocity is updated in a manner that conserves momentum pairwise. In this paper we analyze this model, furthering the understanding of the relationship of the model parameters with the dynamic properties of the system such as the mean squared displacement (MSD) and the shear relaxation modulus. We discuss additional insights that we have developed, particularly related to the friction coefficient associated with the background fluid. We have also derived an approximate expression for the mean squared displacement of the coarse-grained particles for a simple case of non-interacting particles.

Although initially developed independently by Padding and Briels,[26] the momentum conserving algorithm bears similarity to an existing modeling technique called Smoothed Dissipative Particle Dynamics (SDPD),[32] which also incorporates thermal fluctuations in the standard SPH approach. SDPD has been shown to obey proper scaling with varying resolution for Brownian motion of a colloidal particle as well as a polymer molecule in suspension.[33] The method has recently been used to simulate polymeric liquids,[34,35] where polymer molecules are represented as linear chains of beads connected to each other with springs in the presence of other fluid elements. The main difference between their approach and ours is that we discretize the Navier-Stokes equation for computing the velocity of the background fluid on the same nodes which also represent the centers-of-mass of the coarse-grained polymer molecules, thereby making our approach computationally more efficient. It is also worth mentioning that several improvements that have been suggested to SDPD, like incorporating angular momentum conservation,[36,37] can also be easily incorporated in our technique if it is employed for applications where this might be important.[38]

The discussion so far has been restricted to bulk flow, i.e., flow in the absence of interfaces or in other words, flow occurring in the bulk far away from any interfaces. If the algorithm is to be applied to study the flow of soft matter systems through confined spaces involving solid interfaces, then it is also necessary to impose appropriate boundary conditions at the solid-fluid interfaces, which is an important objective of the work that we present here. There is significant ongoing work in this direction. Several techniques for implementing

boundary conditions for coarse-grain techniques such as smoothed particle hydrodynamics and dissipative particle dynamics have been developed.[39–42] We have used the technique of incorporating randomly placed "artificial particles" in the wall and implementing boundary conditions used by Morris *et al.*[39] for modeling low Reynolds number incompressible flows using smoothed particle hydrodynamics. The choice of the term "artificial particles" here is simply motivated by the fact that these particles do not obey any real dynamics. Rather, the sole function of these artificial particles is to offer friction to the real fluid particles in the vicinity of the wall by acting like "frozen particles." However the position of these artificial particles is not fixed in the wall. In order that the real particles feel a uniform wall, i.e., to ensure that the random positions of these artificial particles in the wall do not bias the flow field in any way, the position of these artificial particles is constantly randomized within the wall. This obviates the need to use a high density of these particles in order to maintain the uniformity of the wall. Thus, we present a technique for modeling flow of complex soft matter fluids using a Galilean invariant algorithm in the presence of solid interfaces.

II. MODEL DEVELOPMENT

A. Update of positions

The equation of motion for the mesoscopic particle i in a moving background using Brownian dynamics is given by

$$\mathrm{d}\mathbf{R}_i(t) = \mathbf{v}_i(t)\mathrm{d}t + \frac{\mathbf{F}_i(t)}{\xi_i}\mathrm{d}t + k_BT\frac{\partial}{\partial \mathbf{R}_i}\left(\frac{1}{\xi_i}\right)\mathrm{d}t + \mathrm{d}\mathbf{W}_i^R(t), \quad (1)$$

where we must clarify that the first term on the right hand side of the above equation, i.e., $\mathbf{v}_i(t)$, is not the velocity of the mesoscopic particle i itself; rather it is the velocity of the background material at the position of the mesoscopic particle, relative to which the particle experiences friction. The second term on the right hand side denotes the contribution from the overall force $\mathbf{F}_i$ experienced by the particle i including the external force field as well as the interaction with other mesoscopic particles. It must be noted that the friction coefficient ξ_i has been assumed to be a constant in this paper for the sake of simplicity, thereby obviating the need to account for its positional variation shown in the third term on the right hand side. The fourth term on the right hand side, i.e., $\mathrm{d}\mathbf{W}_i^R(t)$ is a random displacement typical of Brownian dynamics simulations. The properties of the random fluctuations in the position updates are calculated based on the fluctuation dissipation theorem and are thus defined as follows:

$$\langle \mathrm{d}\mathbf{W}_i^R \mathrm{d}\mathbf{W}_j^R \rangle = \frac{2k_BT}{\xi_i}\delta_{ij}\mathrm{d}t\mathbf{I}. \quad (2)$$

B. Update of velocities

If the background flow field is known *a priori*, then it can be plugged into Eq. (1) and the problem can be solved quite easily. However, the flow field for soft matter fluids flowing through complex geometries is typically quite complex and is not known *a priori*. To calculate the background flow field based on the motion of the coarse grain coordinates, we use the momentum conserving Galilean invariant two-way coupling scheme proposed by Padding and Briels[26] with our own modifications. This algorithm couples the motion of the coarse-grain coordinates and the background flow field with each other. In this section, we briefly describe this algorithm and its development. The scheme for updating velocities in this algorithm is not based on a microscopic description but rather a phenomenological description. Consider the Navier-Stokes equation for the velocity field $\mathbf{v}(\mathbf{r})$ of a Newtonian liquid having kinematic viscosity ν,

$$\frac{\mathrm{D}\mathbf{v}}{\mathrm{D}t}(\mathbf{r}) = \nu\nabla^2\mathbf{v}(\mathbf{r}) + \mathbf{g}(\mathbf{r}), \quad (3)$$

where $\mathrm{D}/\mathrm{D}t$ is the material derivative and $\mathbf{g}(\mathbf{r})$ is the acceleration due to body forces. Now, instead of solving the above equation on an Eulerian grid, inspired by Smoothed Particle Hydrodynamics (SPH),[27–31] we calculate the velocity of the background material only at the positions of the particles, which is where it is actually needed as can be seen from Eq. (1). Thus, we have

$$\frac{\mathrm{D}\mathbf{v}}{\mathrm{D}t}(\mathbf{R}_i) = \frac{\mathrm{d}\mathbf{v}_i}{\mathrm{d}t}. \quad (4)$$

The acceleration due to body forces for the background fluid is due to the force $\mathbf{F}_i$ acting on the coarse-grained particles, which is immediately transmitted to the background fluid using an effective mass m_i as follows:

$$\mathbf{g}(\mathbf{R}_i) = \frac{\mathbf{F}_i}{m_i}. \quad (5)$$

For calculating the Laplacian of the velocity field, i.e., $\nabla^2\mathbf{v}(\mathbf{r})$, a finite-difference like form has been employed, which is a symmetrized version of the form originally proposed by Brookshaw.[43] Thus, we have

$$\nu\nabla^2\mathbf{v}(\mathbf{R}_i) = \nu\sum_{j=1}^{N} m_j\left(\frac{1}{\rho_i} + \frac{1}{\rho_j}\right)\left(\mathbf{v}_i - \mathbf{v}_j\right)\frac{1}{R_{ij}}\frac{\mathrm{d}w}{\mathrm{d}r}(R_{ij}), \quad (6)$$

where R_{ij} is the distance between particles i and j, the function $w(r)$ is a normalized dimensionless weight function defined later, and ρ_i is the effective mass density for the background fluid in the vicinity of particle i defined as follows:

$$\rho_i = \frac{\sum_{j=1}^{N} m_j w(R_{ij})}{1 + w(0)/\rho^{\#}}, \quad (7)$$

where the sum in the numerator includes the self term $j = i$. We must point out that we have changed the definition of ρ_i from the original definition proposed in the algorithm by Padding and Briels[26] in order to ensure proper normalization[44] so that for a homogeneous solution, we have $\rho = m\rho^{\#}$, where $\rho^{\#}$ is the number density of the particles.

Putting together Equations (3)–(6) and including a random term as per the fluctuation dissipation theorem, we arrive at the following equation that we have used in our simulations for the update of the velocities:

$$\mathrm{d}\mathbf{v}_i(t) = \frac{\mathbf{F}_i(t)}{m_i}\mathrm{d}t + \sum_{j=1}^{N}\frac{f_{ij}}{\tau}(\mathbf{v}_j(t) - \mathbf{v}_i(t))\mathrm{d}t + \sum_{j=1}^{N}\mathrm{d}\mathbf{W}_{ij}^{v}, \quad (8)$$

where f_{ij}, which is shorthand for $f(R_{ij})$, is a normalized dimensionless weight function and τ is a characteristic time constant

associated with the background fluid, both of which will be defined later, such that their ratio is given by

$$\frac{f_{ij}}{\tau} = -\nu\, m_j \left(\frac{1}{\rho_i} + \frac{1}{\rho_j}\right) \frac{1}{R_{ij}} \frac{\mathrm{d}w}{\mathrm{d}r}(R_{ij}) \qquad (r \le R_c). \tag{9}$$

The last term on the right hand side of Eq. (8) is a random contribution to the velocity update, defined pairwise in an anti-symmetric manner such that $m_i \mathrm{d}\mathbf{W}^v_{ij} = -m_j \mathrm{d}\mathbf{W}^v_{ji}$ so that the velocity updates are momentum conserving. The properties of these velocity fluctuations $\mathrm{d}\mathbf{W}^v_{ij}$ have been calculated in a way that the probability distribution of the coarse-grain coordinates and velocities at a steady state matches with the expected equilibrium distribution. For a detailed derivation starting with the Chapman-Kolmogorov equations leading to a Fokker-Planck equation for the evolution of the probability distribution, we refer to the appendix of the paper by Padding and Briels.[26] Accordingly, we have

$$\left\langle \mathrm{d}\mathbf{W}^v_{ij} \mathrm{d}\mathbf{W}^v_{ij} \right\rangle = \frac{2k_BT}{m_i} \frac{f_{ij}}{\tau} \mathrm{d}t\mathbf{I}, \tag{10}$$

$$\left\langle \mathrm{d}\mathbf{W}^v_{ik} \mathrm{d}\mathbf{W}^v_{jl} \right\rangle = \mathbf{0} \qquad (ik \neq jl \wedge ik \neq lj), \tag{11}$$

$$\left\langle \mathrm{d}\mathbf{W}^R_{i} \mathrm{d}\mathbf{W}^v_{jk} \right\rangle = \mathbf{0}. \tag{12}$$

If we multiply Eq. (8) throughout by the effective mass m_i, we obtain

$$m_i \mathrm{d}\mathbf{v}_i(t) = \mathbf{F}_i(t)\mathrm{d}t + \sum_{j=1}^{N} f_{ij} \frac{m_i}{\tau} (\mathbf{v}_j(t) - \mathbf{v}_i(t))\mathrm{d}t + m_i \sum_{j=1}^{N} \mathrm{d}\mathbf{W}^v_{ij}. \tag{13}$$

Owing to the resemblance of the above rearranged equation with the Langevin equation, we naturally define the friction coefficient associated with the background fluid in an analogous manner as follows:

$$\xi'_i = \frac{m_i}{\tau}. \tag{14}$$

It must be noted that in our simulations, all the particles have an identical mass and hence the friction coefficient ξ'_i has been assumed to be a constant in this paper. However, contrary to the paper by Padding and Briels,[26] we do not set ξ' identically equal to ξ. Rather, in this paper, we have investigated the effect of this friction coefficient ξ' on the dynamics of the system, which is actually very significant. The numerical value for ξ' can be indirectly calculated based on the value of the mass, which can be calculated as the ratio of the mass density of the system to the number density of the particles and the value of the characteristic time constant, which can be calculated based on the kinematic viscosity of the system, as will be clear later. In this paper, however, since our focus is model development, we have not used real values obtained from experimental data but rather non-dimensionalized our results with respect to a basis set, which will be defined later.

C. Interaction with solid walls

For studying confined flows, i.e., flows in the presence of solid interfaces, it is important to take into account the interaction of the fluid with the solid walls establishing appropriate boundary conditions. We have tested our model for applying the no-slip boundary conditions with a test case where we have a star polymer solution flowing between two infinite, parallel solid walls. Our model for the solid-fluid interactions consists of incorporating "artificial" particles in the wall and implementing Morris boundary conditions,[39] which provide the necessary friction to the real particles in order to obtain no-slip boundary conditions at the solid-fluid interface. The Morris boundary conditions involve assigning an artificial velocity to these artificial particles for every pairwise interaction with a real particle, such that the interpolated velocity at the solid interface is zero. This is achieved by setting the artificial velocity of an artificial particle B at a perpendicular distance d_B from the solid interface for its interaction with a real particle A at a perpendicular distance d_A from the solid interface as follows:

$$\mathbf{v}_B = -(d_B/d_A)\mathbf{v}_A. \tag{15}$$

It must be emphasized that this is an artificial velocity and this velocity is not used to evolve the position of the artificial particle. Rather, it is used for calculating the difference in the velocity of the particles needed for the velocity update of the real particle, as follows:

$$\mathbf{v}_A - \mathbf{v}_B = \beta \mathbf{v}_A, \tag{16}$$

where the value of β is restricted with an upper bound for practical considerations for the eventuality that the particle A may approach very close to the solid-fluid boundary, as follows:

$$\beta = min\left(\beta_{max}, 1 + \frac{d_B}{d_A}\right), \tag{17}$$

where β_{max} is chosen to be 1.5 in our simulations as suggested by Morris *et al.*[39] Furthermore, the velocity fluctuation term for the interaction between real and artificial particles is also augmented with a factor of $\sqrt{\beta}$, which prevents cooling of the fluid near the wall. The positions of the artificial particles within the wall are selected randomly at every time step in order to maintain the uniformity of the wall. This has proven to be very effective, thus obviating the need for using a higher density of these artificial particles inside the wall which would have been computationally more intensive. So in our simulations, we have chosen the density of artificial particles embedded in the wall to be the same as the density of the real particles. Besides, we also use a repulsive potential which keeps the real particles from penetrating into the wall, which is the region in which the artificial particles are distributed. For the repulsive potential, we have chosen a Gaussian function with two parameters as follows:

$$\phi^{rep}(r_i) = a\ \exp\left(-b\, r_i^2\right), \tag{18}$$

where r_i is the perpendicular distance of particle i from a plane situated within the wall at a distance of 1.2σ from the interface, a is a parameter chosen to be 300 k_BT, and b is a parameter chosen to be $2\sigma^{-2}$. These parameters have been selected such that the real particles do not penetrate the 1.5σ thick wall embedded with artificial particles on the top and bottom of the channel of width 10σ in which the real particles are present.

III. TEST SYSTEM AND PARAMETERS

A. Test system

We have tested our model with a star polymer solution at the overlap concentration. The behavior of star polymers can vary ranging from ultrasoft to nearly hard colloid like behavior as their interpenetrability depends on their functionality, which is defined as the number of linear chains (arms) bound to the central core of the star polymer. Owing to their wide-ranging interactions, they can be used to study a range of colloidal properties for different interactions.[45] At an intermediate functionality, due to the radial variation of the monomer concentration,[46] each star polymer can be treated as a soft repulsive sphere with a small central core and a corona of grafted chains around it. We use a potential V_{ss} for the interaction between the particles in our simulation, which has been used for modeling star polymers in the past and has also been verified by scattering experiments.[7] It is defined as follows:

$$\frac{V_{ss}(r)}{k_BT} = \frac{5}{18}f^{3/2}\left[-\ln\left(\frac{r}{\sigma}\right) + \frac{1}{1+\sqrt{f}/2}\right] \qquad \text{for } r \le \sigma \tag{19}$$

$$= \frac{5}{18}f^{3/2}\frac{1}{1+\sqrt{f}/2}\frac{\sigma}{r}\exp\left[-\frac{\sqrt{f}}{2\sigma}(r-\sigma)\right] \qquad \text{for } \sigma < r \le r_c, \tag{20}$$

where f is the functionality, r is the distance between the particles, σ is the effective corona diameter, and r_c is the cut-off radius at which the potential is truncated, which is chosen such that the forces are negligible beyond this distance.

B. Definitions of weight functions and the characteristic time constant

We have chosen a normalized weight function $w(r)$ from the SPH literature that smoothly decays to zero as r approaches the cut-off radius R_c, given as follows:

$$w(r) = \frac{21}{2\pi R_c^3}\left(1-\frac{r}{R_c}\right)^4\left(4\frac{r}{R_c}+1\right) \qquad (r \le R_c). \tag{21}$$

Thus, in accordance with Eqs. (9) and (21), we define the normalized weight function f_{ij} and the characteristic time constant τ as follows:

$$f_{ij} = -\frac{R_c^2}{28}m_j\left(\frac{1}{\rho_i}+\frac{1}{\rho_j}\right)\frac{1}{R_{ij}}\frac{\mathrm{d}w}{\mathrm{d}r}(R_{ij}) \qquad (r \le R_c), \tag{22}$$

$$\tau = \frac{R_c^2}{28\nu}, \tag{23}$$

where the coefficient $R_c^2/28$ appears due to normalization of f_{ij}. Simplifying further, we obtain the following expression for f_{ij}:

$$f_{ij} = \frac{15}{2\pi R_c^3}m_j\left(\frac{1}{\rho_i}+\frac{1}{\rho_j}\right)\left(1-\frac{R_{ij}}{R_c}\right)^3 \qquad (r \le R_c). \tag{24}$$

C. Parameter values

We have expressed all the variables in terms of a basis set consisting of the following three quantities: (1) thermal energy k_BT, (2) diffusion coefficient D_o, and (3) effective corona diameter σ. The friction coefficient ξ is assumed to be constant for the sake of simplicity and is given by $\xi = k_BT/D_0$. Furthermore, we have also assumed a uniform mass which implies a uniform ξ' for all the particles in any given simulation. However we have performed simulations with different values of ξ' by systematically varying the ratio ξ'/ξ ranging from 1 to 100. We have used a time step $\mathrm{d}t = 10^{-4}\sigma^2/D_0$ for all our simulations. We have performed several simulations with different values of τ ranging form $1.0\times10^{-3}\sigma^2/D_0$ to $1.0\times10^{1}\sigma^2/D_0$ ensuring that we always maintain $\tau > 10\,\mathrm{d}t$ for stability of the algorithm. In our simulations, we have worked with star polymers having a functionality $f = 128$. For operating at the overlap concentration ($c = c^*$), the number density of the star polymers has been fixed to 0.24 σ^{-3}.[47] For the confined flow simulations, the density of artificial particles inside the wall is the same as the density of the real particles. So in a cubical simulation box having a side of 13 σ, we have 524 particles. We have used an effective cut-off radius $r_c = 2.5\,\sigma$ for the potential beyond which the forces are weak enough to be ignored. We have chosen the same cut-off distance R_c for our weight function $w(r)$ as well, which leads to approximately 15 particles within a sphere of radius R_c, ensuring that we have an accurate enough estimate of the Laplacian of the velocity field.

IV. RESULTS AND DISCUSSION

A. Bulk flow simulations in a quiescent state

In this section, we present the results for simulations of our test system, i.e., a star polymer solution at overlap concentration performed in the absence of any solid interfaces to simulate flows far away from any walls, i.e., in the bulk, in a quiescent state. We have studied the effect of our model parameters on some static and dynamic properties of the system and compared the results with standard Brownian dynamics simulations in the absence of a background flow field (referred to as "standard BD" in the graphs). All the static properties remain unaffected by the Galilean invariant algorithm.[26] As can be seen from Fig. 1, we have verified that the radial distribution function $g(r)$ of the particles for several different values of the parameters of the algorithm is identical to the radial distribution function of the particles in the absence of a background flow field.

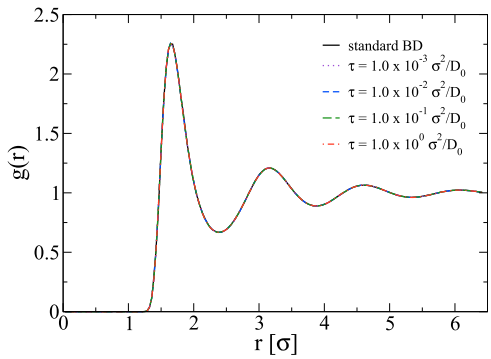

FIG. 1. Radial distribution function of the particles obtained from the standard Brownian dynamics simulation shown with black solid line vs. Brownian dynamics with the Galilean invariant algorithm for various values of the parameter τ (for any given value of ξ'/ξ) shown with colored dotted lines.

It is interesting to note however that even though the static properties are unaffected by the Galilean invariant algorithm, we have found that the dynamic properties are affected by it. We have studied the effect on two dynamic properties, viz., the shear relaxation modulus $G(t)$ and the mean squared displacement (MSD) of the particles by a systematic variation of the system parameters τ and ξ'. We have found that the effect on the dynamic properties due to variation of τ is significant and directly depends on the value of ξ' or vice versa. Since we have implicitly chosen ξ as a basic unit as it is directly linked to D_0, we will discuss this effect in terms of the ratio ξ'/ξ. The shear relaxation modulus $G(t)$ has been computed as an autocorrelation of spontaneous shear stress fluctuations in an equilibrium simulation, as shown in the following equations:

$$G(t) = \frac{V}{k_B T}\left\langle S_{xy}^{pp}(t) S_{xy}^{pp}(0)\right\rangle, \tag{25}$$

$$S_{xy}^{pp}(t) = -\frac{1}{V}\sum_{i<j}\left(x_i - x_j\right) F_{y,ij}, \tag{26}$$

where V denotes the volume of the box and S_{xy}^{pp} is the xy-component of the microscopic particle stress tensor which is calculated from $F_{y,ij}$, the y-component of the force on particle i due to its interaction with particle j. The effect of the model parameters on the shear relaxation modulus $G(t)$ of the particles is shown in Fig. 2.

The mean squared displacement has been calculated as follows:

$$\mathrm{MSD}(t) = \left\langle (\mathbf{r}(t) - \mathbf{r}(0))^2 \right\rangle. \tag{27}$$

The effect of the model parameters on the mean squared displacement (MSD) of the particles is shown in Fig. 3.

It can be observed from the graphs of the shear relaxation modulus $G(t)$ as shown in Fig. 2 that the higher the value of τ, the slower the stresses relax until eventually approaching the standard Brownian dynamics limit at very high values of τ. Furthermore, the effect of variation of τ is more pronounced for smaller values of the ratio ξ'/ξ and it becomes almost insignificant at high values of the ratio ξ'/ξ. A similar effect can be seen for the mean squared displacement of the particles. As can be seen from Fig. 3, the long term diffusion coefficient decreases with increasing value of τ until finally approaching the standard Brownian dynamics limit at very high values of τ. Again, as in the case of the shear relaxation modulus, the effect is more pronounced at smaller values of the ratio ξ'/ξ and becomes almost insignificant at higher values of the ratio ξ'/ξ.

The effect of τ on the dynamic properties can be readily understood if we interpret τ as being indicative of the time over which the background velocity is averaged or in other words, the memory of the system. If we rewrite Eq. (8) using Eq. (14) and assume a homogeneous distribution of particles, we get

$$\mathbf{v}_i(t+\mathrm{d}t) = \left(1 - \frac{\mathrm{d}t}{\tau}\right)\mathbf{v}_i(t) + \frac{\mathrm{d}t}{\tau}\left[\frac{\mathbf{F}_i(t)}{\xi}\left(\frac{\xi'}{\xi}\right)^{-1} + \sum_{j=1}^{N} f_{ij}\mathbf{v}_j(t)\right] + \sum_{j=1}^{N}\mathrm{d}\mathbf{W}_{ij}^{v}. \tag{28}$$

From this perspective, the background velocity in the vicinity of particle i can be interpreted as being calculated based on spatio-temporal averaging.[26] Clearly, the characteristic time constant τ dictates over how many time steps the system will average the background velocity or in other words what is the memory of the system. So if τ is very large, the background velocity gets averaged over such a long time that it becomes effectively negligible since we are dealing with the bulk in a quiescent state (i.e., the velocities fluctuate about a long term average value of zero). The position updates then reduce to standard Brownian dynamics.

Another interesting point here is that this effect of τ on the dynamic properties systematically diminishes as the value

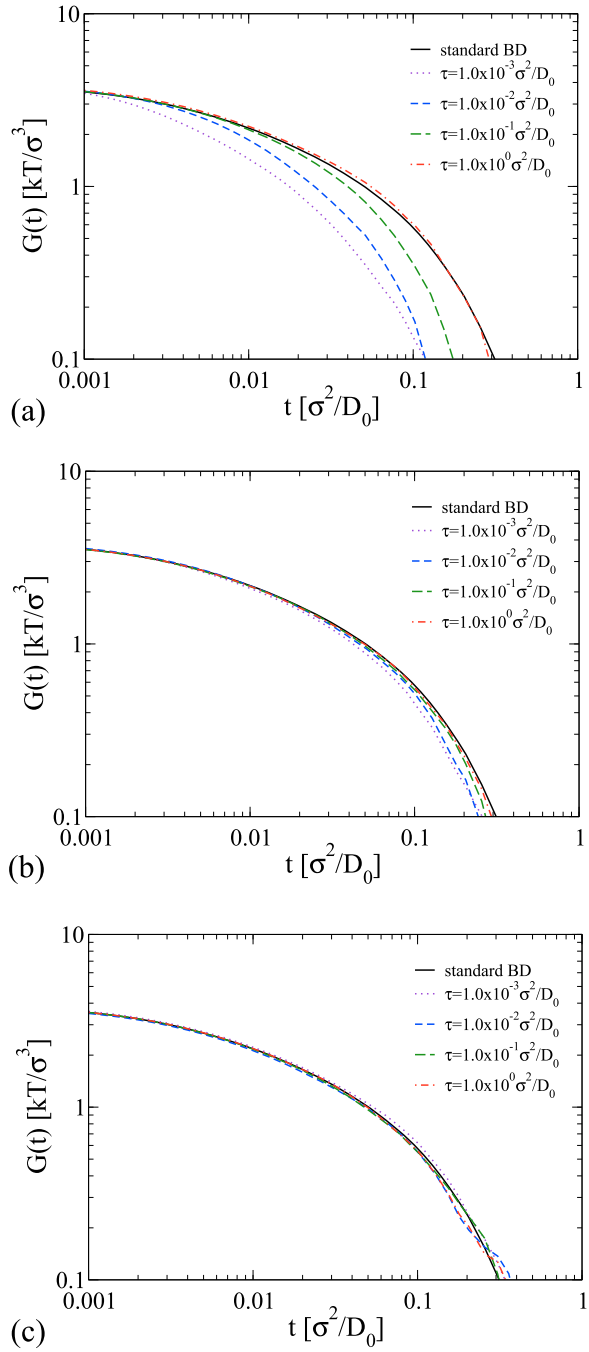

FIG. 2. Shear relaxation modulus of the particles using the standard Brownian dynamics simulation shown with black solid line vs. using the Galilean invariant algorithm for various parameter values shown with colored dotted lines. (a) $\xi'/\xi = 1$, (b) $\xi'/\xi = 10$, (c) $\xi'/\xi = 100$.

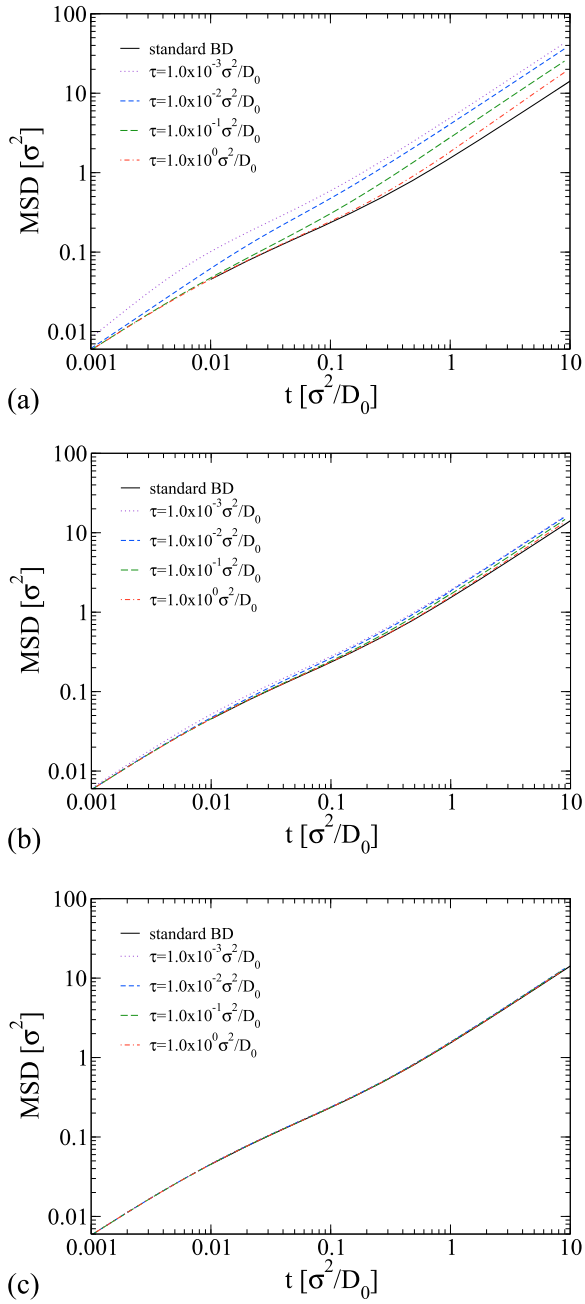

FIG. 3. Mean squared displacement of the particles using standard Brownian dynamics simulation shown with black solid line vs. using the Galilean invariant algorithm for various parameter values shown with colored dotted lines. (a) $\xi'/\xi = 1$, (b) $\xi'/\xi = 10$, (c) $\xi'/\xi = 100$.

of the ratio ξ'/ξ is increased, until finally becoming almost insignificant at very large values of the ratio ξ'/ξ. This is due to the fact that when $\xi' \gg \xi$, the coupling between the coarse grain motion and the background flow field becomes insignificant which can be seen from Eq. (28) as the diminishing effect of the force transmitted to the background flow field when ξ'/ξ is very large. In other words, when the ratio ξ'/ξ is very large, the background flow field does not feel the interactions between the coarse-grain particles and vice versa, leading to the shear relaxation modulus and the mean squared displacement of the particles approaching the standard Brownian dynamics limit.

The model is thus very general and can be used for a diverse range of behaviors ranging from particles that are strongly affected by the fluctuations of the background to particles that are so weakly affected by the fluctuations of the background that they are almost oblivious of its existence. Since the diffusion coefficient is something that can be measured for a system experimentally, it could be used to calculate the parameters of the model. Therefore, we next derive an approximate expression for the mean squared displacement. It must be pointed out however that this derivation is approximate in the sense that it does not fully capture the effects due to all the model parameters, as it makes several assumptions.

Consider a simple case of non-interacting particles in the bulk in a quiescent state, i.e., a case where there are no forces on the particles except for the random kicks and velocity fluctuations. For a homogeneous solution where the friction coefficients of all particles are identical, the model dictates the following position and velocity updates, respectively:

$$\mathrm{d}\mathbf{R}_i(t) = \mathbf{v}_i(t)\mathrm{d}t + \mathrm{d}\mathbf{W}_i^R(t), \tag{29}$$

$$\mathrm{d}\mathbf{v}_i(t) = \frac{1}{\tau}\sum_{j=1,j\neq i}^{N} f_{ij}\mathbf{v}_j(t)\mathrm{d}t - \frac{\mathbf{v}_i(t)\mathrm{d}t}{\tau}\sum_{j=1,j\neq i}^{N} f_{ij} + \sum_{j=1,j\neq i}^{N}\mathrm{d}\mathbf{W}_{ij}^v(t). \tag{30}$$

For a homogeneous solution, $\sum_{j=1,j\neq i}^{N} f_{ij}$ averaged over a long time would be equal to unity for all particles. So as a simplifying assumption, we assume a constant average value of $\sum_{j=1,j\neq i}^{N} f_{ij} = 1$, thereby also neglecting any correlations that it may have with the velocities. The above equation then can be alternatively written as an integral equation as follows:

$$\mathbf{v}_i(t) = \mathbf{v}_i(0)e^{-t/\tau} + \int_0^t \mathrm{d}t' e^{-(t-t')/\tau} \times\left(\sum_{j=1,j\neq i}^{N}\frac{\mathrm{d}\mathbf{W}_{ij}^v(t')}{\mathrm{d}t} + \frac{1}{\tau}\sum_{j=1,j\neq i}^{N} f_{ij}\mathbf{v}_j(t')\right). \tag{31}$$

This equation may be solved in the usual way by iteration. Actually, since the second term in the integrand will be small, we expect that the zeroth order calculation by neglecting this term will give a good result. For a detailed derivation, the reader may refer to the Appendix. For the zeroth order calculation, we arrive at the following result:

$$\langle\Delta\mathbf{R}_i(t)^2\rangle = \frac{6k_BT}{\xi'_i}\left[t - \tau\left(1 - e^{-t/\tau}\right)\right] + \frac{6k_BT}{\xi_i}t. \tag{32}$$

After a sufficiently long time, i.e., $t \gg \tau$, we get

$$\langle\Delta\mathbf{R}_i(t)^2\rangle = \frac{6k_BT}{\xi'_i}t + \frac{6k_BT}{\xi_i}t. \tag{33}$$

Thus, we can see from the above equation that the effect of the friction coefficient associated with the background on the dynamic properties of the system such as the mean squared displacement of the particles is significant and is in line with what we observed from the simulation results shown earlier. We can use Eq. (33) to set the value of the friction coefficient ξ so as to obtain the correct diffusion coefficient of the particles in the system.

In order to compare our derivation results, we have performed simulations of particles with the potential V_{ss} turned off so as to be as close to the assumptions made in the derivation as possible and the results are shown in Fig. 4.

As we can see from Fig. 4, the expression derived from theory satisfactorily predicts the mean squared displacement of the particles, particularly for large values of τ.

B. Flow simulations with solid interfaces

To test the model for flow in the presence of solid interfaces, we have performed simulations of the test system, i.e., a star polymer solution flowing through a rectangular channel. The cubical simulation box with each side measuring 13 σ consists of a rectangular channel of width 10 σ that has been simulated by having two walls filled with artificial particles, each of thickness 1.5 σ, placed within the box—one at the top and the other at the bottom. Periodic boundary conditions have been applied in all the directions including the vertical direction so that any particle approaching a wall effectively encounters a wall of 3 σ, which is more than the cut-off radius R_c of 2.5 σ. This prevents any unrealistic interactions a particle near the bottom wall could have had with another particle near the top wall due to the periodic boundary conditions in the vertical direction. Alternatively, one can also have a wall of 2.5 σ thick on the top and the bottom face without periodic boundary conditions in the vertical direction but this would involve using a greater number of artificial particles. In the simulations, flow has been induced in the positive x-direction by using a gravity field g, which is essentially applied by applying a constant force F_x to all the particles in the positive x-direction. Now, this force may be applied to the particles and transmitted to the background fluid or alternatively the gravity field may just be applied to the background fluid through the force term in the update of the velocities without using it in the update of the positions. In either approach, similar velocity profiles are obtained. Here, we present the results for the case where the force F_x is applied to the particles and transmitted to the background fluid.

In the simulation results that we have presented in this section, we have non-dimensionalized the density, velocity, and temperature profiles. The density profile has been non-dimensionalized using the bulk density ρ^{bulk}, which is essentially the ratio of the total mass of all particles to the total volume of the box. It is important to note that the density of the artificial particles within the channel is the same as the density of the real particles in the channel, which is equal to ρ^{bulk}. The velocity profile is calculated by dividing the box into 26 slabs and measuring the velocities of all the particles within each slab. We are mainly interested in the component of the velocity in the direction of the flow, which in our simulations was the positive x-direction. So, for each slab, the distribution of x-component of the velocities is calculated from a histogram, which is populated by the x-component of the velocities of all the particles in that slab. We run the simulation for 10^7 time steps and use the last 9×10^6 time steps for populating the histogram for measurement of the velocity distribution.

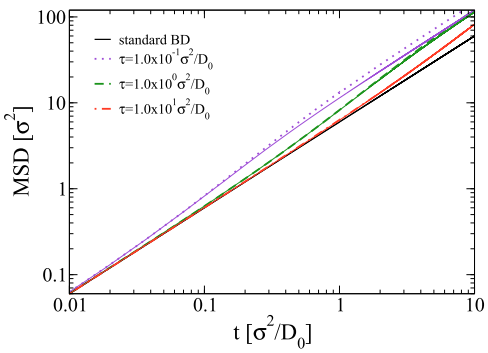

FIG. 4. Comparison of the mean squared displacement of the non-interacting particles using the result from the derivation, i.e., Eq. (32) with simulations for $\xi'/\xi = 1$. The colored dotted lines are simulation results, the colored solid lines are the analytical approximations from the derivation, and the black solid line is for a standard Brownian dynamics simulation.

The mean of the velocity distribution generated by the histograms of each slab is then assigned as the velocity associated with that slab, which is how each point on the velocity profiles shown in this section has been calculated. We have then non-dimensionalized the velocity profile thus generated using the basis set units. The temperature is calculated from the standard deviation of the velocity distributions generated by the histogram of each slab, as we expect a Maxwellian distribution of the velocities which entails a normal distribution of each of the velocity components with a standard deviation of $\sqrt{k_BT/m}$. We have then non-dimensionalized this temperature profile with the desired temperature T_0, which was an input to the simulations.

For the sake of comparison, we have also performed similar simulations with a commercial CFD package COMSOL Multiphysics 5.0.[48] For a proper comparison, it is important that we must input the correct physical properties of our test fluid, particularly the viscosity of the fluid. So we performed independent bulk shear-flow simulations with our particle-based model based on the Lees-Edwards method,[49] whereby we modify the periodic boundary conditions as follows. Assume that in a box of height L_y, the top wall moves with a velocity of $\dot{\gamma}L_y/2$ in the x-direction and the bottom wall moves with a velocity of $-\dot{\gamma}L_y/2$ in the x-direction. When a particle crosses the bottom boundary and arrives at the top of the box, it is displaced by $\dot{\gamma}Lt$ in the x-direction and the background velocity at the position of the particle is augmented by $\dot{\gamma}L$. Alternatively, if a particle crosses the top boundary and arrives at the bottom of the box, it is displaced by $-\dot{\gamma}Lt$ in the x-direction and the background velocity at the position of the particle is augmented by $-\dot{\gamma}L$. Moreover, during the force calculation, if a particle interacts with its neighbor across the boundary, then the background velocity of the neighboring particle is adjusted by $\pm\dot{\gamma}L$ depending on whether the neighbor is in the bottom or the top of the box. The viscosity from these simulations is then calculated as the ratio of the average stress S_{xy} based on Eq. (26) and the shear rate $\dot{\gamma}$. This is the particle-contribution of the shear viscosity to which we must add the background fluid contribution, which we will discuss later. We fitted the flow curve thus obtained from these simulations with the Carreau equation,[50] given as follows:

$$\frac{\eta - \eta_\infty}{\eta_0 - \eta_\infty} = \left[1 + (\lambda\dot{\gamma})^2\right]^{\frac{n-1}{2}}, \tag{34}$$

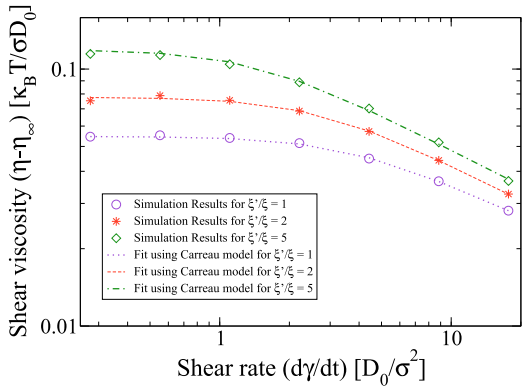

FIG. 5. Flow curve obtained from shear flow simulations for different values of ξ'/ξ and $\tau = 3 \times 10^{-3}\ \sigma^2/D_0$ based on the Lees-Edwards method shown with the colored symbols and the fit using the Carreau model shown with the colored dotted lines.

where η_0 is the zero shear rate viscosity, η_∞ is the infinite shear viscosity, λ is a parameter with units of time, and n is a dimensionless parameter. The shear viscosity without the infinite shear viscosity component $(\eta - \eta_\infty)$ is fitted with the Carreau model optimizing the three parameters, i.e., $(\eta_0 - \eta_\infty)$, λ, and n, as shown in Fig. 5.

Approximating the infinite shear viscosity η_∞ as the background fluid viscosity, an estimate for η_∞ can be obtained in terms of our model parameters as follows:

$$\eta_\infty = \frac{R_c^2 \rho^{\#} \xi'}{28}. \tag{35}$$

We have performed our flow simulations through a channel using a constant gravity field $g = F_x/m$, which must be translated to the analogous pressure drop per unit length of the channel for the corresponding COMSOL simulations. The relation between the pressure drop per unit length $\Delta P/L_x$ and our model parameters has been defined as follows:

$$\Delta P/L_x = F_x \rho^{\#}. \tag{36}$$

Furthermore, we have assumed Stokes flow for the COMSOL simulations, thereby neglecting inertial terms from the Navier-Stokes equations. In Fig. 6, we have shown the comparison of the results for the flow of our test system of a star polymer solution through a rectangular channel obtained from the simulations based on our model with the results from the corresponding COMSOL simulations for a shear thinning fluid obeying the Carreau model. The three sub-figures (a)–(c)

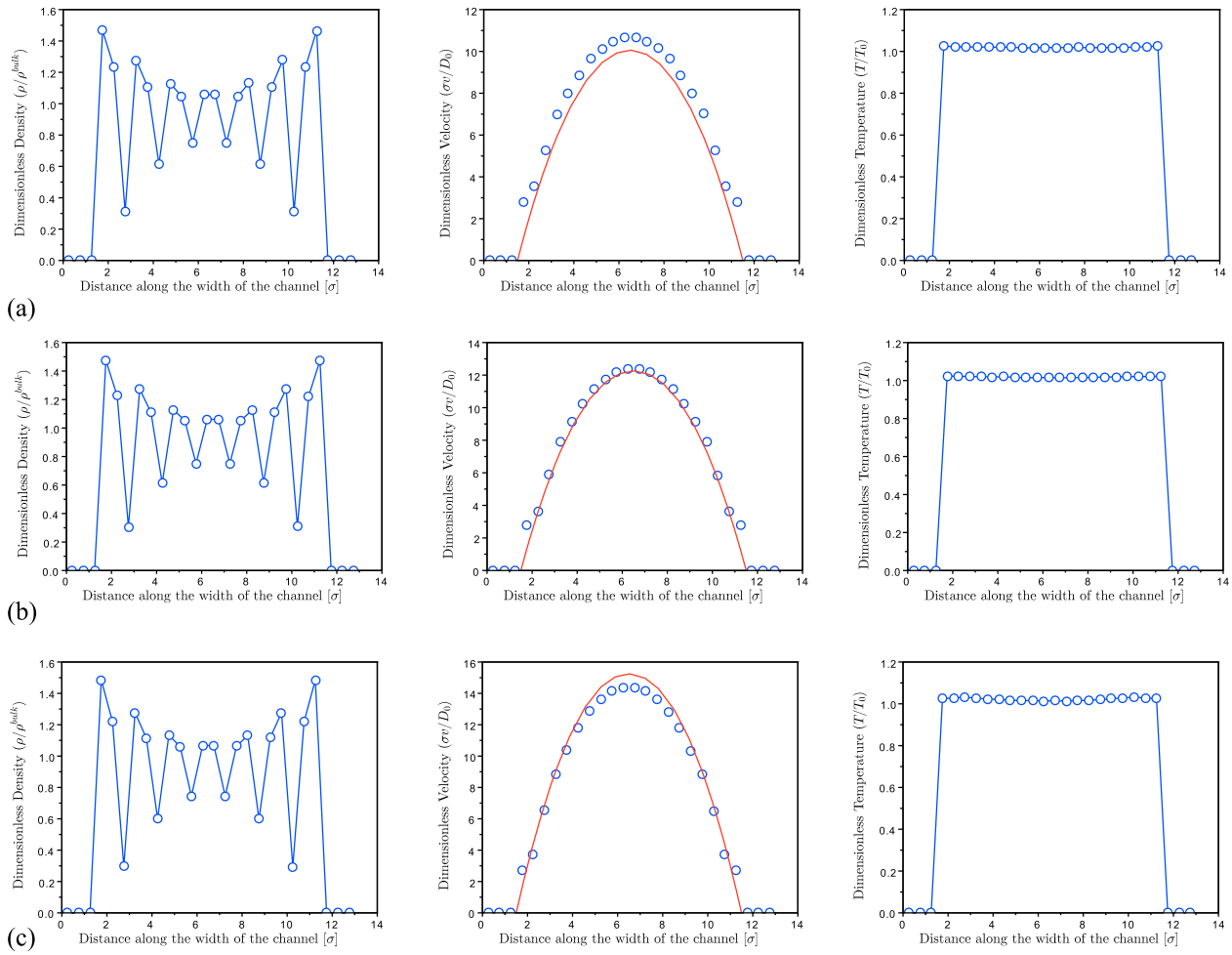

FIG. 6. Dimensionless density, velocity, and temperature profiles for different parameter values using the Morris boundary conditions. The velocity profile shown with circles is obtained from particle based simulations based on our model and the solid line shows the results from COMSOL simulations for a shear thinning fluid following the Carreau equation. (a) $\xi'/\xi = 1$ for $\tau = 3 \times 10^{-3}\ \sigma^2/D_0$. (b) $\xi'/\xi = 2$ for $\tau = 3 \times 10^{-3}\ \sigma^2/D_0$. (c) $\xi'/\xi = 5$ for $\tau = 3 \times 10^{-3}\ \sigma^2/D_0$.

of Fig. 6 show the results of the simulations performed for three different values of ξ', viz., 1, 2, and 5, respectively, for a constant value of $\tau = 3 \times 10^{-3}\ \sigma^2/D_0$ and maintaining a constant gravity field $g = F_x/m = 133.4D_0^2/\sigma^3$ by scaling forces F_x proportional to ξ'. Each of the sub-figures of Fig. 6 shows the dimensionless density profile on the left, the dimensionless velocity profile in the center, and the dimensionless temperature profile on the right.

As can be seen from Fig. 6, the temperature is uniform throughout the cross section and is close to its expected value that was set as an input value T_0, which is the same value used for normalization. The density profiles correspond to the test system that we have employed. We see a layered fluid owing to the nature of the potential and the presence of a hard wall. This was to be expected looking at the radial distribution function from Fig. 1 and the hard wall potential shown in Eq. (18). The dimensionless velocity profiles agree satisfactorily with the profiles obtained from the COMSOL simulations for several parameter values. It is also interesting to note that despite the pronounced density fluctuations, we have obtained a rather smooth velocity profile. This is because the cut-offs for the normalized weight functions w_{ij} and f_{ij} used to calculate the average local properties and their gradients, respectively, have been chosen in such a way that we have about 15 particles within the cut-off, which effectively smooths out the fluctuations due to the density profile.

It must be pointed out that the range of values for the parameters we have chosen is in such a way that the maximum particle Reynolds number is less than 1. An estimate for the particle Reynolds number can be obtained by solving the Navier-Stokes equation for a Newtonian fluid with a viscosity ν which is related to the parameters by Eq. (23). The maximum velocity in the channel of width L_y for the flow of a Newtonian fluid with viscosity ν under the influence of a gravity field g is as follows:

$$v_{max} = \frac{gL_y^2}{8\nu}. \tag{37}$$

Accordingly, the maximum particle Reynolds number is as follows:

$$Re_{max} = \frac{\sigma g L_y^2}{8\nu^2}. \tag{38}$$

Using Eqs. (38) and (23), we arrive at the following condition on the parameters:

$$98\frac{\sigma g \tau^2}{R_c^2}\left(\frac{L_y}{R_c}\right)^2 < 1. \tag{39}$$

In other words, we get an upper bound of $5.47 \times 10^{-3}\sigma^2/D_0$ for the value of τ. Accordingly, we have used a value of $3 \times 10^{-3}\sigma^2/D_0$ for the channel flow simulations.

V. CONCLUSION AND SCOPE FOR FURTHER RESEARCH

In this paper, we have presented a technique for modeling flow of highly frictional soft matter systems in the presence of solid interfaces. The technique is largely based on a Galilean invariant coupling algorithm,[26] which we have modified and then thoroughly analyzed to its further understanding. We have demonstrated the relationship of the modelparameters with the dynamic properties of the system. Furthermore, we have also presented an iterative procedure to theoretically predict the effect of the friction coefficients on the mean squared displacement for a simple case of non-interacting particles, which can be used to then determine the values of the system parameters. We have presented the model in a very generalized manner so that it may be applied to a wide range of systems by tuning the parameters of the model.

It must however be pointed out that for highly viscous systems, the time step required for the velocity propagator introduced by the Galilean invariant algorithm can be much smaller than the time step required for the position updates based on Brownian dynamics. Thus, for such systems, it might be practical to use a multiscale approach where two different time steps are used for the position and velocity updates. A large number of velocity updates can be carried out before the positions of the particles change significantly. Alternatively, a steady state solution may be calculated for the velocities every time the positions are updated.

Furthermore, it must be noted that although using the particles as the nodes on which the background flow field is discretized makes the model computationally efficient, the resolution of the background fluid is actually limited by the concentration of the particles in the system. For instance, in the case of a star polymer solution, the concentration of the polymers fixes the resolution of the background fluid because the particles play dual roles of representing the star polymers and also being the node points on which the background flow field is discretized. This may be resolved by having a model with two types of particles—ones representing the polymer particles and the others representing the background fluid, but for this case, correctly describing the interaction between the two types of particles is crucial.

ACKNOWLEDGMENTS

This work is part of the Industrial Partnership Programme (IPP) "Computational sciences for energy research" of the Foundation for Fundamental Research on Matter (FOM), which is part of the Netherlands Organisation for Scientific Research (NWO). This research programme is co-financed by Shell Global Solutions International B.V.

APPENDIX: MEAN SQUARED DISPLACEMENT OF NON-INTERACTING PARTICLES

In this section, we present the zeroth order calculation for mean squared displacement mentioned in Sec. IV A. For the zeroth order calculation, we neglect the second term in the integrand on the right hand side of Eq. (31). Substituting the result into Eq. (29) and integrating, we get the displacement as

$$\Delta\mathbf{R}_i(t) = \mathbf{v}_i(0)\int_0^t \mathrm{d}t' e^{-t'/\tau} + \int_0^t \mathrm{d}t' \int_0^{t'} \mathrm{d}t'' e^{-(t'-t'')/\tau} \times \sum_{j=1, j\neq i}^{N} \frac{\mathrm{d}\mathbf{W}_{ij}^v(t'')}{\mathrm{d}t} + \int_0^t \mathrm{d}t' \frac{\mathrm{d}\mathbf{W}_i^R(t')}{\mathrm{d}t}. \tag{A1}$$

Making use of $\int_0^t \mathrm{d}t' \int_0^{t'} \mathrm{d}t'' = \int_0^t \mathrm{d}t'' \int_{t''}^t \mathrm{d}t'$ and performing some integrations, we get

$$\Delta\mathbf{R}_i(t) = \tau\mathbf{v}_i(0)\left(1 - e^{-t/\tau}\right) + \tau\int_0^t \mathrm{d}t'\left(1 - e^{-(t-t')/\tau}\right)\sum_{j=1,j\neq i}^{N}\frac{\mathrm{d}\mathbf{W}_{ij}^v(t')}{\mathrm{d}t} + \int_0^t \mathrm{d}t'\frac{\mathrm{d}\mathbf{W}_i^R(t')}{\mathrm{d}t}. \tag{A2}$$

Squaring and averaging the above equation over the ensemble, and noting that the random variables have a zero mean and noting further that the random variables associated with the positions and velocities are uncorrelated with each other as defined in Eq. (12), we get

$$\langle\Delta\mathbf{R}_i(t)^2\rangle = \tau^2\left(1 - e^{-t/\tau}\right)^2\langle\mathbf{v}_i(0)^2\rangle + \tau^2\int_0^t \mathrm{d}t'\int_0^t \mathrm{d}t''\left\{(1 - e^{-(t-t')/\tau})(1 - e^{-(t-t'')/\tau})\right.$$
$$\left.\sum_{j=1,j\neq i}^{N}\sum_{k=1,k\neq i}^{N}\left\langle\frac{\mathrm{d}\mathbf{W}_{ij}^v(t')}{\mathrm{d}t}\cdot\frac{\mathrm{d}\mathbf{W}_{ik}^v(t'')}{\mathrm{d}t}\right\rangle\right\} + \int_0^t \mathrm{d}t'\int_0^t \mathrm{d}t''\left\langle\frac{\mathrm{d}\mathbf{W}_i^R(t')}{\mathrm{d}t}\cdot\frac{\mathrm{d}\mathbf{W}_i^R(t'')}{\mathrm{d}t}\right\rangle. \tag{A3}$$

In order to evaluate this equation further, we make use of

$$\langle\mathbf{v}_i(0)^2\rangle = \frac{3k_BT}{m_i}, \tag{A4}$$

$$\left\langle\frac{\mathrm{d}\mathbf{W}_{ij}^v(t')}{\mathrm{d}t}\cdot\frac{\mathrm{d}\mathbf{W}_{ik}^v(t'')}{\mathrm{d}t}\right\rangle = \frac{6k_BT}{m_i}\frac{f_{ij}}{\tau}\delta_{jk}\delta(t' - t''), \tag{A5}$$

$$\left\langle\frac{\mathrm{d}\mathbf{W}_i^R(t')}{\mathrm{d}t}\cdot\frac{\mathrm{d}\mathbf{W}_i^R(t'')}{\mathrm{d}t}\right\rangle = \frac{6k_BT}{\xi_i}\delta(t' - t''). \tag{A6}$$

Here we have used that fact the random terms at different times are uncorrelated, in which case $\delta_{t't''}/\mathrm{d}t = \delta(t' - t'')$. Using the definition of mass given in Eq. (14), and simplifying, we obtain the expression for the mean squared displacement based on our zeroth iteration as follows:

$$\left\langle\Delta\mathbf{R}_i(t)^2\right\rangle = \frac{6k_BT}{\xi_i'}\left[t - \tau(1 - e^{-t/\tau})\right] + \frac{6k_BT}{\xi_i}t. \tag{A7}$$

After a sufficiently long time, i.e., $t \gg \tau$, we get

$$\langle\Delta\mathbf{R}_i(t)^2\rangle = \frac{6k_BT}{\xi_i'}t + \frac{6k_BT}{\xi_i}t. \tag{A8}$$

[1] D. C. Rapaport, *The Art of Molecular Dynamics Simulation* (Cambridge University Press, 2004).
[2] M. P. Allen and D. J. Tildesley, *Computer Simulation of Liquids* (Oxford University Press, 1989).
[3] G. A. Voth, *Coarse-Graining of Condensed Phase and Biomolecular Systems* (CRC Press, 2008).
[4] M. Karttunen, I. Vattulainen, and A. Lukkarinen, *Novel Methods in Soft Matter Simulations* (Springer Science & Business Media, 2004), Vol. 640.
[5] M. Murat, and K. Kremer, J. Chem. Phys., **108**, 4340 (1998).
[6] R. D. Groot and P. B. Warren, J. Chem. Phys. **107**, 4423 (1997).
[7] C. N. Likos, H. Löwen, M. Watzlawek, B. Abbas, O. Jucknischke, J. Allgaier, and D. Richter, Phys. Rev. Lett., **80**, 4450 (1998).
[8] A. Van den Noort, W. K. den Otter, and W. J. Briels, Europhys. Lett., **80**, 28003 (2007).
[9] I. S. Santos de Oliveira, A. van den Noort, J. T. Padding, W. K. den Otter, and W. J. Briels, J. Chem. Phys., **135**, 104902 (2011).
[10] I. S. Santos de Oliveira, W. K. den Otter, and W. J. Briels, J. Chem. Phys., **137**, 204908 (2012).
[11] P. J. Hoogerbrugge and J. M. V. A. Koelman, Europhys. Lett., **19**, 155 (1992).
[12] J. M. V. A. Koelman and P. J. Hoogerbrugge, Europhys. Lett., **21**, 363 (1993).
[13] P. Espanol and P. Warren, Europhys. Lett., **30**, 191 (1995).
[14] W. Briels, *Theory of Polymer Dynamics* (Uppsala, Sweden, 1994).
[15] C. W. Gardiner *et al.*, *Handbook of Stochastic Methods* (Springer, Berlin, 1985), Vol. 4.
[16] E. Frey and K. Kroy, Ann. Phys., **14**, 20 (2005).
[17] S. Izvekov and G. A. Voth, J. Chem. Phys., **125**, 151101 (2006).
[18] C.-C. Huang, H. Xu, F. Crevel, J. Wittmer, and J.-P. Ryckaert, *Computer Simulations in Condensed Matter Systems: From Materials to Chemical Biology* (Springer, 2006), Vol. 2, pp. 379–418.
[19] I. S. Santos de Oliveira, B. W. Fitzgerald, W. K. den Otter, and W. J. Briels, J. Chem. Phys., **140**, 104903 (2014).
[20] I. M. Ilie, W. K. den Otter, and W. J. Briels, J. Chem. Phys., **141**, 065101 (2014).
[21] E. S. Boek, J. T. Padding, V. J. Anderson, W. J. Briels, and J. P. Crawshaw, J. Non-Newtonian Fluid Mech. **146**, 11 (2007).
[22] J. T. Padding, E. S. Boek, and W. J. Briels, J. Chem. Phys., **129**, 074903 (2008).
[23] A. Van den Noort and W. J. Briels, J. Non-Newtonian Fluid Mech. **152**, 148 (2008).
[24] J. Sprakel, E. Spruijt, J. van der Gucht, J. T. Padding, and W. J. Briels, Soft Matter **5**, 4748 (2009).
[25] J. Sprakel, J. T. Padding, and W. J. Briels, Europhys. Lett., **93**, 58003 (2011).
[26] J. T. Padding and W. J. Briels, J. Chem. Phys., **141**, 244108 (2014).
[27] R. A. Gingold and J. J. Monaghan, Mon. Not. R. Astron. Soc., **181**, 375 (1977).
[28] L. B. Lucy, Astron. J **82**, 1013 (1977).
[29] R. Gingold and J. Monaghan, J. Comput. Phys. **46**, 429 (1982).
[30] J. J. Monaghan, Annu. Rev. Astron. Astrophys., **30**, 543 (1992).
[31] J. J. Monaghan, Rep. Prog. Phys., **68**, 1703 (2005).
[32] P. Espanol and M. Revenga, Phys. Rev. E, **67**, 026705 (2003).
[33] A. Vázquez-Quesada, M. Ellero, and P. Español, J. Chem. Phys., **130**, 034901 (2009).
[34] S. Litvinov, M. Ellero, X. Hu, and N. A. Adams, Phys. Rev. E, **77**, 066703 (2008).
[35] S. Litvinov, Q. Xie, X. Hu, N. Adams, and M. Ellero, Fluids, **1**, 7 (2016).
[36] X. Hu and N. Adams, Phys. Fluids **18**, 101702 (2006).
[37] K. Müller, D. A. Fedosov, and G. Gompper, J. Comput. Phys., **281**, 301 (2015).
[38] I. O. Götze, H. Noguchi, and G. Gompper, Phys. Rev. E, **76**, 046705 (2007).
[39] J. P. Morris, P. J. Fox, and Y. Zhu, J. Comput. Phys., **136**, 214 (1997).
[40] M. Revenga, I. Zuniga, and P. Espanol, Comput. Phys. Commun., **121**, 309 (1999).
[41] I. V. Pivkin and G. E. Karniadakis, J. Comput. Phys. **207**, 114 (2005).
[42] J. Smiatek, M. P. Allen, and F. Schmid, Eur. Phys. J. E, **26**, 115 (2008).
[43] L. Brookshaw, Proc. Astron. Soc. **6**, 207 (1985).

[44] For a homogeneous solution, $\sum_{j=1,j\neq i}^{N} w(R_{ij}) = \int d^3r\rho^{\#}w(r) = \rho^{\#}$, and hence, $\sum_{j=1}^{N} mw(R_{ij}) = m\left(w(0) + \sum_{j=1,j\neq i}^{N} w(R_{ij})\right) = m\rho^{\#}(1 + w(0)/\rho^{\#})$, from which the result follows.

[45]D. Vlassopoulos and G. Fytas, *High Solid Dispersions* (Springer, 2009), pp. 1–54.
[46]M. Daoud and J. Cotton, J. Phys., **43**, 531 (1982).
[47]J. T. Padding, E. Van Ruymbeke, D. Vlassopoulos, and W. J. Briels, Rheol. Acta, **49**, 473 (2010).
[48]Comsol, Multiphysics User Guide for COMSOL 5.0, 2014.
[49]A. Lees and S. Edwards, J. Phys. C: Solid State Phys., **5**, 1921 (1972).
[50]R. Bird, W. Stewart, and E. Lightfoot, *Transport Phenomena*, Wiley International Edition (Wiley, 2007).